Monthly Notices
of the
ROYAL ASTRONOMICAL SOCIETY

Mon. Not. R. Astron. Soc. **401,** 362–370 (2010) doi:10.1111/j.1365-2966.2009.15647.x

Counterstreaming magnetized plasmas with kappa distributions – II. Perpendicular wave propagation

M. Lazar,[1,2⋆] R. C. Tautz,[2⋆] R. Schlickeiser[2⋆] and S. Poedts[1⋆]

[1] *Center for Plasma Astrophysics, Celestijnenlaan 200B, 3001 Leuven, Belgium*
[2] *Institut für Theoretische Physik, Lehrstuhl IV: Weltraum- und Astrophysik, Ruhr-Universität Bochum, D-44780 Bochum, Germany*

Accepted 2009 September 1. Received 2009 September 1; in original form 2009 July 16

ABSTRACT

The analysis of the stability and the dispersion properties of a counterstreaming plasma system with kappa distributions are extended here with the investigation of perpendicular instabilities. Purely growing filamentation (Weibel-like) modes propagating perpendicular to the background magnetic field can be excited in streaming plasmas with or without an excess of parallel temperature. In this case, however, the effect of suprathermal tails of kappa populations is opposite to that obtained for parallel waves: the growth rates can be higher and the instability faster than for Maxwellian plasmas. The unstable wavenumbers also extend to a markedly larger broadband making this instability more likely to occur in space plasmas with anisotropic distributions of kappa-type. The filamentation instability of counterstreaming magnetized plasmas could provide a plausible mechanism for the origin of two-dimensional transverse magnetic fluctuations detected at different altitudes in the solar wind.

Key words: plasmas – waves – methods: analytical.

1 INTRODUCTION

Non-thermal particle distributions are ubiquitous at high altitudes in the solar wind, their presence being widely confirmed by measurements aboard spacecrafts (Montgomery, Bame & Hundhausen 1968; Feldman et al. 1975; Pilipp et al. 1987; Maksimovic, Pierrard & Riley 1997a; Zouganelis 2008). The suprathermal populations have been described for the first time by Vasyliunas (1968) using the so-called kappa (κ-) velocity distribution functions (VDFs). These are power laws in particle speed and with high-energy tails deviated from a Maxwellian. For a counterstreaming plasma system, two kappa-like distributions are shown in fig. 1 from Lazar et al. (2008a), hereafter Paper I.

Various mechanisms have been proposed to explain the origin of the suprathermal tails of the VDFs and the occurrence of kappa-like distributions in the solar wind and corona. In an ambient quasi-static magnetic field, plasma charges gain energy through the cyclotron resonance and the transit time damping (Landau resonance) of linear waves. Thus, the high-frequency whistler modes can enhance the energy of electrons in Earth's foreshock (Ma & Summers 1998), and MHD waves can accelerate both the electrons and the protons in the solar flares (Miller 1991, 1997), and in the inner magnetosphere (Summers & Ma 2000). When large amplitude waves are present, the non-linear Landau damping can be responsible for the energization of plasma particles (Miller 1991; Leubner 2000; Shizgal 2007). The non-thermal features of the VDFs can also result from superdiffusion processes (Treumann 1997) and due to heat flows or the presence of the temperature anisotropies (Leubner & Viñas 1986). An interesting mechanism of velocity filtration (in the solar corona) has also been proposed (Scudder 1992) to explain the high-energy electrons at higher altitudes in the solar wind.

The collisionless or weakly collisional models in the corona (Scudder 1992; Zouganelis et al. 2005), both using VDFs with a suprathermal tail, are able to reproduce the high-speed streams of the fast solar wind emitted out of coronal regions where the plasma temperature is smaller (Maksimovic, Pierrard & Lemaire 1997b; Zouganelis et al. 2005), as well as the low-speed solar wind originating in the hotter equatorial regions of the solar corona (Maksimovic et al. 1997b). On the other hand, the electron VDFs measured at 1 au have been used as boundary condition to determine the VDFs at different altitudes (Pierrard, Maksimovic & Lemaire 1999, 2001), and it was proved that, for several solar radii, the suprathermal populations must be present in the corona as well (Pierrard et al. 1999).

As a result of low collision rates in the interplanetary plasma, the electrons and the ions can develop temperature anisotropies and their VDFs become skewed and develop tails and heat fluxes along the ambient magnetic field (Marsch et al. 1982; Pilipp et al. 1987; Salem et al. 2003; Stverak et al. 2008). Moreover, field-aligned fluxes of (suprathermal) particles can be encountered at any altitude in the solar wind (Pilipp et al. 1990), but they become prominent in energetic shocks, like the coronal mass ejections or the fast solar wind at the planetary bow shock, giving rise to counterstreaming plasma events (Feldman et al. 1974; Gosling et al. 1993). The same

⋆E-mail: Marian.Lazar@wis.kuleuven.be (ML); rct@tp4.rub.de (RCT); rsch@tp4.rub.de (RS); Stefan.Poedts@wis.kuleuven.be (SP)

mechanisms mentioned above can induce anisotropic non-thermal VDFs in counterstreaming plasmas, and such complex plasmas can hold an important amount of free energy that makes them unstable to the excitation of waves and instabilities.

The modified plasma dispersion function is used to analyse the dispersion properties of a hot plasma with kappa-distributed particles (Summers & Thorne 1991; Mace & Helberg 1995). The properties of longitudinal Langmuir and ion acoustic waves have been compared for both distributions, kappa and Maxwellian, finding that the Landau damping of long wavelength Langmuir modes is significantly enhanced for a Lorentzian plasma (Thorne & Summers 1991). This limits the existence of the (weakly damped) Langmuir waves in space plasmas with kappa distributions to a narrow band just above the electron plasma frequency.

In this series of works, we investigate the dispersion properties and the stability of a counterstreaming plasma system with intrinsic anisotropies modelled by a bi-kappa distribution function. Plasma flows are assumed to be naturally streaming along a magnetic guide field. Whereas in Paper I the case of parallel wave propagation was studied, here we investigate the waves propagating perpendicular to the magnetic field. Streaming plasmas or an excess of parallel temperature can destabilize the ordinary mode propagating perpendicular to the background magnetic field. The instability readily arises in plasmas with large parallel beta ($\beta_\parallel = 8\pi n_0 k_B T_\parallel / B_0^2$), when the parallel kinetic energy is much greater than the magnetic confinement energy. Due to the presence of streaming, the instability can, however, occur in low-β plasmas as well (Bornatici & Lee 1970) and it may then play a role in pulsars, magnetostars or plasma experiments.

2 COUNTERSTREAMING DISTRIBUTION FUNCTION

In order to describe the counterstreaming plasma system with intrinsic temperature anisotropies of bi-kappa-type, we reload the general form of the unperturbed particle VDF chosen in Paper I:

$$f_\kappa = \frac{1}{\pi^{3/2}\theta_\perp^2\theta_\parallel}\,\frac{\Gamma(\kappa+1)}{\kappa^{3/2}\Gamma(\kappa-1/2)} \times\left\{\epsilon_1\left[1+\frac{(v_\parallel-v_1)^2}{\kappa\theta_1^2}+\frac{v_\perp^2}{\kappa\theta_\perp^2}\right]^{-\kappa-1} +\epsilon_2\left[1+\frac{(v_\parallel+v_2)^2}{\kappa\theta_2^2}+\frac{v_\perp^2}{\kappa\theta_\perp^2}\right]^{-\kappa-1}\right\}. \quad (1)$$

This is normalized as $\int \mathrm{d}^3v\, f_\kappa = 1$. We keep the significance and notation for all the quantities used in Paper I: the polar components of particle velocity

$$(v_x, v_y, v_z) = (v_\perp\cos\phi, v_\perp\sin\phi, v_\parallel); \quad (2)$$

the bulk velocities $v_{1,2}$; the perpendicular and parallel thermal velocities

$$v_{\mathrm{T}_\perp}^2 = \frac{k_B T_\perp}{m}; \quad v_{\mathrm{T}_{1,2}}^2 = \frac{k_B T_{1,2}}{m}, \quad (3)$$

which give

$$\theta_\perp = \left(\frac{2\kappa-3}{\kappa}\right)^{1/2} v_{\mathrm{T}_\perp} \quad (4)$$

and

$$\theta_\parallel = \epsilon_1\theta_1 + \epsilon_2\theta_2 = \left(\frac{2\kappa-3}{\kappa}\right)^{1/2}(\epsilon_1 v_{\mathrm{T}_1} + \epsilon_2 v_{\mathrm{T}_2}); \quad (5)$$

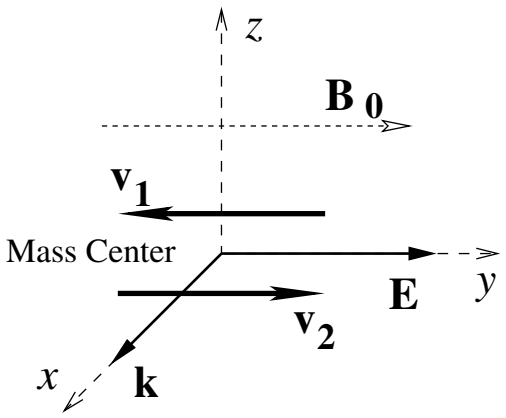

Figure 1. Two plasma counterstreams with bulk velocities $v_{1,2}$, and the ordinary mode with $\boldsymbol{E}\|\boldsymbol{B}_0$.

and the relative intensities of the counterstreaming plasmas is given by $\epsilon_{1,2} = \omega_{p1,2}/(\omega_{p1}+\omega_{p2})$, where $\omega_{p1,2} = (4\pi n_{1,2}q^2/m)^{1/2}$ are the plasma frequencies of the two counterstreams.

3 PERPENDICULAR WAVE DISPERSION

The streams are aligned with the stationary magnetic field, $\boldsymbol{B}_0$ (parallel to y-axis in Fig. 1), and the unstable plasma modes propagate perpendicular to the magnetic field, ($\boldsymbol{k} \perp \boldsymbol{B}_0$), along the x-axis (in Fig. 1). The general dispersion relation of the perpendicular modes, for an arbitrary distribution function, has been provided in different forms several decades ago [see e.g. Bornatici & Lee (1970) or Davidson (1983) for a non-relativistic plasma, or Cary et al. (1981) for a relativistic plasma response]. A number of weakly relativistic analyses of Bernstein modes propagating perpendicular or nearly perpendicular to the uniform magnetic field in a Maxwellian plasma have shown a relativistic frequency downshift (with a transverse Doppler effect larger than that of the parallel motion) leading to a smearing out of the gyroresonances at high harmonics (see e.g. Robinson 1988 and references therein). However, for anisotropic distributions with a surplus of free energy along the magnetic field the dispersion relation for the ordinary mode admits an additional aperiodic Weibel-like solution, and although a realistic description requires for a relativistic treatment, the quantitative differences for the Weibel instability are minimal (Schaefer-Rolffs & Schlickeiser 2006). Therefore, the non-relativistic equations are appropriate, provided that both the thermal and the streaming velocities are small compared to the speed of light.

The equivalence of the non-relativistic dispersion relations used by Bornatici & Lee (1970) and Davidson (1983) has recently been proven in Tautz & Schlickeiser (2006), and below we will use the simple general forms found there.

3.1 Ordinary mode instability

The ordinary mode, which is a transverse wave with its electric field linearly polarized in the direction of $\boldsymbol{B}_0$, is the only wave mode affected by the presence of a counterstream and a temperature anisotropy (Tautz & Schlickeiser 2006). We therefore expect in this case to obtain a cumulative filamentation/Weibel instability driven by the counterstreaming motion of plasma (filamentation instability) as well as the intrinsic temperature anisotropy of each plasma stream (Weibel instability).

For the ordinary mode, the general dispersion relation is given by (Tautz & Schlickeiser 2006)

$$D_y = 1 - \frac{k^2c^2 + \sum_a \omega_{p,a}^2}{\omega^2} + \sum_a \frac{\omega_{p,a}^2}{\omega^2} \sum_{n=-\infty}^{\infty} \int \mathrm{d}^3 v \, \frac{n\Omega_a \, J_n^2(z_a)}{\omega - n\Omega_a} \frac{v_\parallel^2}{v_\perp} \frac{\partial f_a}{\partial v_\perp} = 0, \quad (6)$$

where

$$z_a = \frac{k v_\perp}{\Omega_a}, \quad (7)$$

and $J_n(z)$ denotes the Bessel function of the first kind of order n. The geometry for this mode is shown in Fig. 1: the polarization is transverse, as $\boldsymbol{k} = k\hat{\boldsymbol{e}}_x$. Here, ω and k are, respectively, the frequency and the wavenumber of the plasma modes, c is the speed of light in vacuum, $\Omega_a = q_a B_0/(m_a c)$ is the (non-relativistic) gyrofrequency and $\omega_{p,a} = (4\pi n_a e^2/m_a)^{1/2}$ is the plasma frequency for the particles of sort a ($a = e$ for electrons and $a = p$ for protons). For the sake of simplicity, in what follows we will neglect the contribution of ions, which form the neutralizing background, and the electron plasma counterstreams are considered homogeneous as well as charge and current neutral.

According to Lerche (1966), equation (6) can be simplified to

$$D_y = 1 - \frac{k^2c^2 + \omega_{p,e}^2}{\omega^2} - \frac{\omega_{p,e}^2}{\omega^2} \int \mathrm{d}^3 v \, [1 + \alpha S(\alpha, z)] \frac{v_\parallel^2}{v_\perp} \frac{\partial f_e}{\partial v_\perp} = 0, \quad (8)$$

where

$$S(\alpha, z) = -\Gamma(\alpha)\Gamma(1-\alpha) J_{-\alpha}(z) J_\alpha(z) \quad (9)$$

and $\alpha = \omega/\Omega_\mathrm{e}$.

3.2 Small gyroradius approximation

The integral in equation (8) can be simplified when the gyroradius of the electrons is much smaller than the wavelength (small gyroradius approximation), and this is shown in Appendix B for two symmetric counterstreaming plasmas. Thus, using equation (B3), the dispersion relation (8) yields

$$\omega^2 - \left(k^2c^2 + \omega_{p,e}^2\right) - \omega_{p,e}^2 \frac{k^2 v_0^2}{\omega^2 - \Omega_\mathrm{e}^2} \left(1 + \frac{v_\mathrm{T}^2}{v_0^2}\right) = 0. \quad (10)$$

Note that in this limit, there is no difference from plasmas with Maxwellian distributions (Tautz & Schlickeiser 2006). Equation (10) corresponds to the classical filamentation (Weibel-like) instability described by Fried (1959) for two cold counterflowing plasmas. Here, equation (10) describes plasma flows with a finite temperature but with a sufficiently small perpendicular thermal velocity $v_{\mathrm{T}_\perp}$, which is not present in the dispersion relation.

Equation (10) admits purely growing solutions with the growth rate

$$\omega_i = \frac{\omega_{p,e}}{\left(k^2c^2 + \omega_{p,e}^2 + \Omega_\mathrm{e}^2\right)^{1/2}} \times \left[k^2\left(v_0^2 + v_\mathrm{T}^2\right) - \Omega_\mathrm{e}^2\left(\frac{k^2c^2}{\omega_{p,e}^2} + 1\right)\right]^{1/2}, \quad (11)$$

and we should remark that in the presence of a static magnetic field, the aperiodic solutions are found for wavenumbers larger than a threshold value imposed by the electron gyrofrequency

$$k > k_\mathrm{t} = \Omega_\mathrm{e}\left(v_0^2 + v_\mathrm{T}^2 - c^2\frac{\Omega_\mathrm{e}^2}{\omega_{p,e}^2}\right)^{-1/2}. \quad (12)$$

For non-magnetized plasmas, this threshold vanishes, $k_\mathrm{t}(\Omega_\mathrm{e} = 0) = 0$. This comes to confirm the recent results of Stockem, Lerche & Schlickeiser (2006) for two cold counterstreaming plasmas, where it was shown that the filamentation instability can grow only for an ambient magnetic field lower than a critical value. Here, this critical value depends on the streaming velocity as well as the parallel thermal velocity as provided by equation (12):

$$B_{0,\mathrm{c}} = \sqrt{4\pi n_0 m_e}\left(v_0^2 + v_\mathrm{T}^2\right)^{1/2}. \quad (13)$$

The unstable solutions exist only for an ambient magnetic field with strength less than this critical value, $B_0 < B_{0,\mathrm{c}}$ (or for sufficiently low $\Omega_\mathrm{e}/\omega_{p,e} < \sqrt{v_0^2 + v_\mathrm{T}^2}/c$). The growth rates given by equation (11) are displayed with the solid line in Fig. 2 for some counterstreaming plasma parameters typically encountered in the solar flares and winds (e.g. the acceleration region of the outer corona). Three different values of $\Omega_\mathrm{e}/\omega_{p,e} = \sqrt{m_p/m_e}(v_\mathrm{A}/c) = 0.01, 0.04, 0.05$ have been chosen to show how the instability depends on the presence of the background magnetic field ($v_\mathrm{A} = B_0/\sqrt{4\pi n_p m_p}$ is the Alfvén speed). The ordinary mode is completely stabilized for intense magnetic fields, for example, in Fig. 2 for $\Omega_\mathrm{e}/\omega_{p,e}$ larger than the critical value $\sim$0.054 given by equation (13).

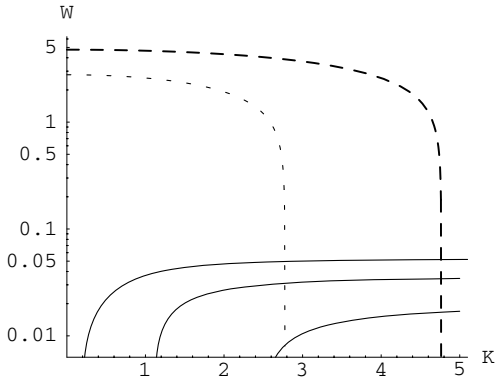

Figure 2. The normalized growth rates, W= $\omega_i/\omega_{p,e}$, as given by equation (11) (solid line), and by equation (17) for $\kappa = 2$ (long-dashed line) and for Maxwellian plasmas (short-dashed line). The parameters chosen for the plasma system are $v_0/c = 0.05$, $v_\mathrm{T}/c = 0.02$ ($T_e \sim 10^6$ K) and $T/T_\perp = 1.2$. For the growth rates given by equation (11), we take $\Omega_\mathrm{e}/\omega_{p,e} = 0.01$, 0.04, and 0.05. The abscissa is scaled as $K = kc/\omega_{p,e}$.

The influence of the ambient magnetic field is noticeable: it tends to suppress the instability by introducing a minimum threshold wavenumber, which is discussed above, and by decreasing the maximum growth rate reached at the saturation:

$$\omega_{i,\max} = \left(\frac{v_0^2 + v_\mathrm{T}^2}{c^2}\omega_{p,e}^2 - \Omega_\mathrm{e}^2\right)^{1/2}. \quad (14)$$

3.3 Large gyroradius approximation

In the opposite limit of a large gyroradius, the integral in equation (6) is calculated in Appendix C. Using equation (C11) in equation (6), we find the following dispersion relation:

$$\frac{\omega^2 - k^2c^2}{\omega_{p,e}^2} + \frac{\theta^2}{\theta_\perp^2}\left[1 + \left(2 - \frac{1}{\kappa}\right)\frac{v_0^2}{\theta^2}\right] = 1. \quad (15)$$

In this case, the ordinary modes become unstable for wavenumbers less than a cut-off value, $k < k_{\rm c}$ given by,

$$k_{\rm c} = \frac{\omega_{p,e}}{c} \left\{ \frac{\theta^2}{\theta_\perp^2} \left[1 + \left(2 - \frac{1}{\kappa} \right) \frac{v_0^2}{\theta^2} \right] - 1 \right\}^{1/2} \tag{16}$$

and has oscillatory frequency negligibly small, $\omega_r \simeq 0$, and the growth rate

$$\omega_i = \omega_{p,e} \left\{ \frac{\theta^2}{\theta_\perp^2} \left[1 + \left(2 - \frac{1}{\kappa} \right) \frac{v_0^2}{\theta^2} \right] - 1 - \frac{k^2 c^2}{\omega_{p,e}^2} \right\}^{1/2}. \tag{17}$$

In this limit, we obtain information about the maximum cut-off wavenumber, $k_{\rm c}$, given in equation (16) that does not rely on the background magnetic field [the cut-off derived here in equation (16) agrees exactly to that obtained for an unmagnetized plasma; see equation (13) in Lazar, Schlickeiser & Shukla (2008b)], but exhibits a strong dependence on the particle velocity anisotropy and the spectral index κ. The growth rates provided by equation (17) are displayed in Fig. 2, with long-dashed line for $\kappa = 2$ and with short-dashed line for Maxwellian plasmas ($\kappa \to \infty$). Here, the critical magnetic field strength derived in equation (13) for very large $k_{\rm t} \to \infty$ must be refined by limiting this threshold to the maximum cut-off $k_{\rm t} = k_{\rm c}$, which yields

$$B_{0,{\rm c}} = \sqrt{4\pi n_0 m_e} \left(v_0^2 + v_{\rm T}^2 \right)^{1/2} \left[1 - \frac{\theta_\perp^2}{\theta^2 + \left(2 - \frac{1}{\kappa} \right) v_0^2} \right]^{1/2}. \tag{18}$$

The correction introduced in equation (18) with respect to equation (13) is, however, a minor one provided that here we assume the perpendicular temperature sufficiently small $\theta_\perp^2 \ll \theta^2 + v_0^2$. For the example chosen in Fig. 2, this correction is indeed very small:

$$\frac{\theta_\perp^2}{\theta^2 + \left(2 - \frac{1}{\kappa} \right) v_0^2} \simeq 0.04 \ll 1.$$

For sufficiently low strengths of the ambient magnetic field, for example much less than the critical values derived above, the effect of the background magnetic field therefore becomes less important (see in Fig. 2), and the instability could be studied by using the following equation:

$$\frac{k^2 c^2}{\omega^2} = 1 + \frac{\omega_{p,e}^2}{\omega^2} \left[\frac{\theta^2}{\theta_\perp^2} - 1 + \frac{\theta^2}{\theta_\perp^2} \frac{\omega}{k\theta_\perp} Z_\kappa^0 \left(\frac{\omega}{k\theta_\perp} \right) \right] + 2 \frac{\omega_{p,e}^2}{\omega^2} \frac{v_0^2}{\theta_\perp^2} \left[\left(1 - \frac{1}{2\kappa} \right) + \frac{\omega}{k\theta_\perp} Z_\kappa \left(\frac{\omega}{k\theta_\perp} \right) \right]. \tag{19}$$

This dispersion relation has been derived by Lazar et al. (2008b) for an unmagnetized counterstreaming plasma with anisotropic kappa-type distributions. In the right-hand side of this equation, the second term includes the contribution of thermal anisotropy while the third term is given by the relative plasma motion. The dispersion equation (19) contains the modified plasma dispersion function (Summers & Thorne 1991)

$$Z_\kappa(f) = \frac{1}{\pi^{1/2} \kappa^{1/2}} \frac{\Gamma(\kappa)}{\Gamma\left(\kappa - \frac{1}{2} \right)} \int_{-\infty}^{+\infty} {\rm d}x \, \frac{(1 + x^2/\kappa)^{-(\kappa+1)}}{x - f}, \quad \Im(f) > 0, \tag{20}$$

and according to Lazar et al. (2008b)

$$Z_\kappa^0(f) = \left(1 + \frac{f^2}{\kappa} \right) Z_\kappa(f) + \frac{f}{\kappa} \left(1 - \frac{1}{2\kappa} \right). \tag{21}$$

Our assertion is confirmed in Fig. 3, where the exact numerical solution of dispersion relation equation (19), the dotted line, approaches quite well the two limit solutions given by equations (11) and (17). Despite the small discrepancy observed for very low wavenumbers due to the presence of the ambient magnetic field, the large cut-off wavenumber provided by the equation (19), $k_{\rm c} = k(\omega = 0)$, fits exactly to that provided by the dispersion relation (17) in equation (16). The dispersion relation (19) can therefore be used to describe the ordinary mode instability with a good accuracy, provided the background magnetic field is weak or the anisotropy is sufficiently large.

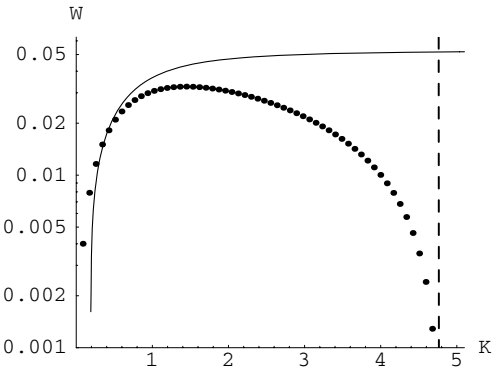

Figure 3. The exact numerical solution of dispersion relation (19), the dotted line, is quite well framed by the two limit solutions given by equation (11), the solid line and equation (17), the dashed line. The parameters are the same as in Fig. 2, and $\Omega_{\rm e}/\omega_{p,e} = 0.01$ is chosen sufficiently low.

We note that in the presence of suprathermal particles the instability extends to large wavenumbers by increasing the maximum cut-off (see the long-dashed line in Fig. 2). This instability is therefore more likely to be present in space plasmas with anisotropic distributions of kappa-type.

4 APPLICATIONS

These instabilities could provide a plausible mechanism for the origin of the two-dimensional transverse magnetic fluctuations observed in the solar wind and flares (Stockem et al. 2006), and can also be responsible for an efficient transfer of the beam energy to the heating of plasma electrons in the direction perpendicular to that of the streams.

4.1 Solar wind

Here, we consider suprathermal counterstreaming beams (with intrinsic temperature anisotropies) expected to arise at different altitudes in the solar wind but predominantly in the outer corona region, where the plasma parameters estimated from the observations are $n_e \sim 10^7$ cm^{-3}, $T_e \sim 10^6$ K. The regular magnetic field is sufficiently weak, $B_0 \sim 0.1$ G, so that $\Omega_{\rm e}/\omega_{p,e} \sim 0.01$, and the ordinary mode instability will be properly described by the dispersion relation (19). The aperiodic solutions of this equation are displayed in the next Figs 4–6 for several representative cases. For comparison with solid line it is shown the solution for the limit Maxwellian case ($\kappa \to \infty$).

Coronal mass ejections and streams can be more or less violent leading to the formation of counterstreaming plasma structures in solar environments. In Fig. 4, we first consider two distinct cases of energetic (but still subrelativistic) electron beams with $v_0 = 0.2c$ (in panel a) and with $v_0 = 0.05c$ (in panel b), and with a moderate temperature anisotropy $T/T_\perp = 2$. In a non-streaming plasma with an

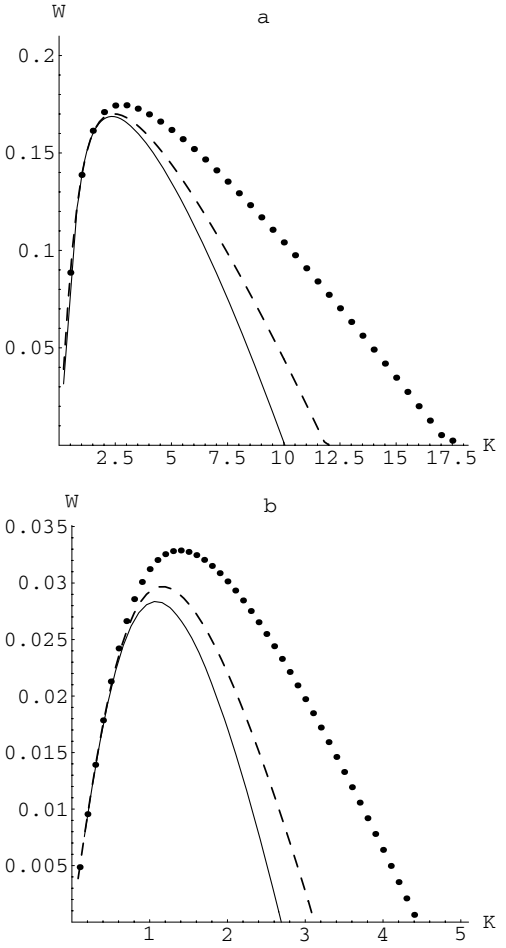

Figure 4. Normalized growth rates, W$=\omega_i/\omega_{p,e}$, as given by equation (19): dotted line for $\kappa = 2$, dashed line for $\kappa = 4$ and solid line for a very large $\kappa \to \infty$ (Maxwellian). The parameters chosen for the plasma system are $\Omega_e/\omega_{p,e} = 0.01$, $v_{T_\perp}/c = 0.02(T_e \sim 10^6\text{K})$, (a) $T/T_\perp = 2$, $v_0/c = 0.2$ and (b) $T/T_\perp = 2$, $v_0/c = 0.05$. The abscissa is scaled as $K = kc/\omega_{p,e}$.

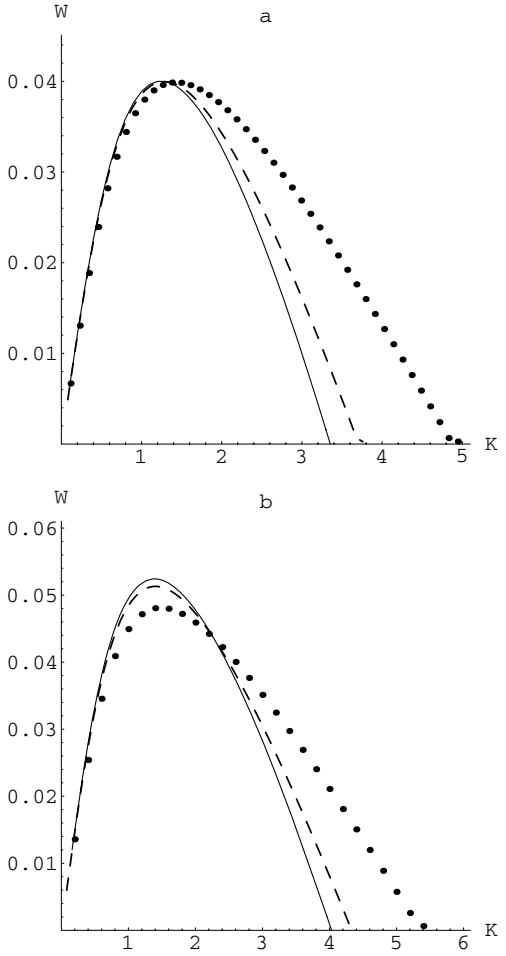

Figure 5. The same as in fig. 4, but for (a) $T/T_\perp = 6$, $v_0/c = 0.05$ and (b) $T/T_\perp = 11$, $v_0/c = 0.05$.

intrinsic thermal anisotropy, the Weibel instability (Weibel 1959) effect is diminished by the presence of the suprathermal populations (Zaheer & Murtaza 2007). In a streaming plasma, the effect of suprathermal particles is opposite, enhancing the growth rates of the filamentation Weibel-like instability (Lazar et al. 2008b). In Fig. 4, we observe that this behaviour is still effective even for streams with moderate intrinsic temperature anisotropies which enhance the instability. But, the effect of suprathermal particles becomes again less important when these anisotropies are higher and dominate the free energy stored in the relative motion of counterstreaming plasmas, and this is shown in Fig. 5. The growth rates become comparable or even smaller, but the thresholds given by the wavenumber cutoff (16) remain more important than that of Maxwellian ($\kappa \to \infty$) plasmas,

$$k_{c,\kappa}^2 - k_{c,\infty}^2 = \frac{v_0^2}{v_{T_\perp}^2}\,\frac{2}{2\kappa - 3} > 0 \qquad (22)$$

so long $v_0 > v_{T_\perp}$. This difference obtained in equation (22) vanishes for less energetic beams with small bulk velocities $v_0 < v_{T_\perp} < v_T$, as can be seen in Fig. 6, and the instability is much faster in the absence of suprathermal populations.

For counterstreams with an excess of parallel temperature, it was shown recently (Lazar et al. 2009b) that the cumulative filamentation/Weibel instability can develop faster than the two-stream electrostatic instability (which is suppressed by the thermal spread of plasma particles). According to this, the counterstreaming plasma structures described by the parameters chosen in Figs 4 and 5 will mainly be destabilized by these instabilities of the Weibel type. Otherwise, if the outflows are observed to be stable this demonstrates

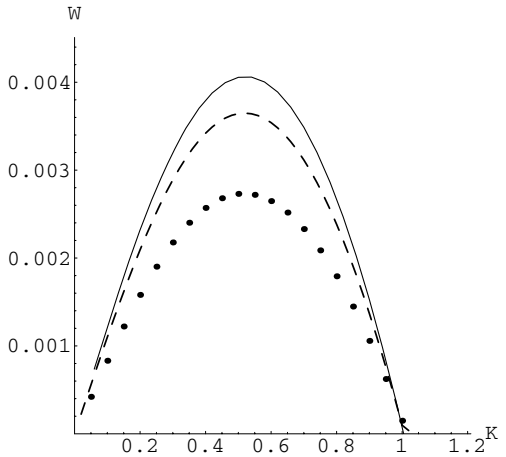

Figure 6. The same as in Fig. 4, but for $T/T_\perp = 2$, $v_0/c = 0.002$. The abscissa is scaled as K$= kc/\omega_{p,e}$.

that plasma is confined moving along the magnetic field lines. In this case, the ambient magnetic field is strong enough to suppress the filamentation instability (in a confined plasma the magnetic energy partially transforms in kinetic energy by increasing the perpendicular temperature and thus diminishing the effective anisotropy of the streaming plasma). The streams are, however, relaxed by the two-stream instability leading to a plateau anisotropic distribution function (with $v_{\rm T} > v_{\rm T_\perp}$). Such anisotropic distributions will again drive an instability of the Weibel type.

4.2 Solar flares

Whereas the streaming flares are observed to be stable in the first precursor or the impulsive stage, in the decay stage, the plasma instabilities can be responsible for their disruption and for releasing the free energy. These solar outflows in flares are most probably in a Maxwellian (collisional) regime, and therefore here we consider the limit case of a sufficiently large $\kappa \gg 1$ that must fit to the Maxwellian dispersion approach of Tautz & Schlickeiser (2006). In this case the dispersion relation of the ordinary mode (8) reduces to [see equation (14) in Tautz & Schlickeiser (2006)]

$$1 = \frac{k^2c^2}{\omega^2} + \frac{\omega_{p,e}^2}{\omega^2}\frac{v_{\rm T}^2 + 2v_0^2}{v_{\rm T_\perp}^2}\left[1 - \hat{F}_e(1)\right], \tag{23}$$

with the short notation for the hypergeometric function

$$\hat{F}_e(1) = {}_2F_2\left(\frac{1}{2}, 1; 1+\alpha, 1-\alpha; -\xi^2\right), \tag{24}$$

where $\alpha = \omega/\Omega_{\rm e}$ and $\xi = k v_{\rm T_\perp}/\Omega_{\rm e}$.

In solar flares, the average values of the plasma parameters cannot be strictly given than only to some limits, $n_e = 10^9$–10^{11} cm^{-3}, $T_e = 10^6 - 10^7$ K. Moreover, the electrons are strongly magnetized (Aschwanden 2004) and can have the gyrofrequency in the interval $\Omega_{\rm e}/\omega_{p,e} = 0.1$–$10$ ($B_0 = 10^2 - 5 \times 10^2$ G). Equation (23) is solved numerically and the purely growing solutions are displayed in Figs 7–9.

In Fig. 7, the growth rates are calculated for isotropic streams with bulk velocity $v_0 = 0.2c$ and different temperatures: $T = 10^7$ K (dashed line), $T = 2 \times 10^6$ K (dot–dashed line) and $T = 10^6$ K (solid line). Note that thermal spread of particles suppresses the instability (which is Weibel-like). In Fig. 8, the growth rates are calculated for anisotropic streams with different intrinsic temperature anisotropies $T/T_\perp = 1, 2$ and 4. Keeping T constant and decreasing

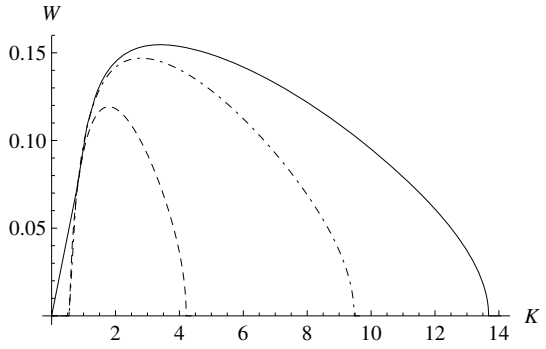

Figure 7. Normalized growth rates, W$= \omega_i/\omega_{p,e}$, as given by equation (23) for isotropic streams with different temperatures: $T = 10^7$ K (dashed line), $T = 2 \times 10^6$ K (dot–dashed line) and $T = 10^6$ K (solid line). The other parameters are $\Omega_{\rm e}/\omega_{p,e} = 0.1$, $v_0 = 0.2c$, and the abscissa is scaled as $K = kc/\omega_{p,e}$.

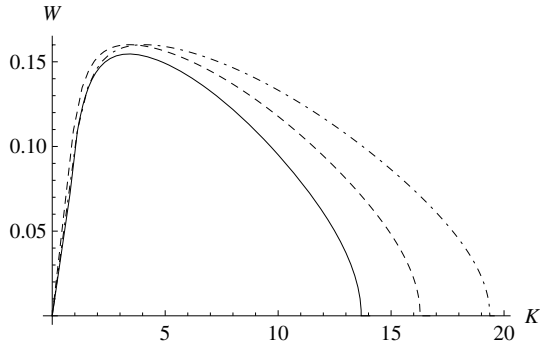

Figure 8. The same as in fig. 7, but for $T = 10^6$ K and anisotropic streams with $T/T_\perp = 1$ (solid line), $T/T_\perp = 2$ (dashed line) and $T/T_\perp = 4$ (dot–dashed line).

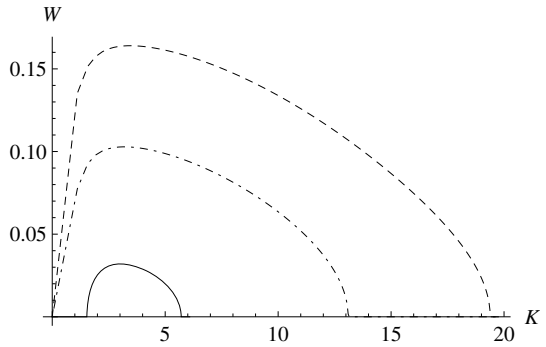

Figure 9. The same as in Fig. 8, but for $T/T_\perp = 4$ and three different bulk velocities $v_0 = 0.2$ (dashed line), $v_0 = 0.15$ (dot–dashed line) and $v_0 = 0.11$ (solid line).

$T_\perp$, the growth rate increases but it is only slightly enhanced by the temperature anisotropy. In Fig. 9, the growth rates are displayed for anisotropic streams, $T/T_\perp = 4$, with different bulk velocities $v_0 =$ 0.20, 0.15 and 0.11. The growth rates decrease and the system is stabilized in the presence of a regular magnetic field if the streaming velocity is not large enough to sustain the instability.

5 DISCUSSION AND CONCLUSION

In this series of two papers, we have examined the effect of suprathermal populations of kappa-type on the dispersion properties of colliding plasma shells frequently invoked in astrophysical scenarios. In the presence of a stationary magnetic field, plasma flows are assumed streaming along this magnetic guide field. We have considered complex counterstreaming plasmas including a finite and anisotropic thermal spread of plasma particles. Thus, the free energy provided by different combinations of the anisotropic velocity distributions of plasma particles cumulates leading either to an enhancing or to a suppression of the wave instability. In addition, here we have shown that these instabilities are markedly altered in kappa-distributed plasmas. In order to be able to handle the mathematics in analytical form, the two limiting cases of wave propagation parallel and perpendicular to the background magnetic field have been investigated. Although in Paper I the case of parallel wave propagation has been investigated, here we have focused on perpendicular wave propagation.

For parallel waves with respect to the regular magnetic field ($\boldsymbol{k} \| \boldsymbol{B}_0$), we have identified two principal branches, the electrostatic two-stream mode developed by the free energy in the

counterstreaming plasma motion and the whistler Weibel-like mode excited by an excess of the transverse temperature. Both instabilities are inhibited by the high-energy tails of the particle distributions leading to lower growth rates with respect to those obtained for Maxwellian plasmas. In the presence of a stationary magnetic field, the Weibel-like instability becomes oscillatory with a finite frequency $\omega_r \neq 0$ (see in fig. 5 from Paper I) but this resonant regime restraints to small wavenumbers in counterstreaming plasmas (see in fig. 4 from Paper I). For energetic flows with a bulk velocity larger than the parallel thermal velocity of plasma particles and an ambient magnetic field negligibly weak, the instability becomes again dominantly resonant (Lazar, Dieckmann & Poedts 2009a). In most of these cases, the phase velocity seems to be too small with respect to the thermal velocity so that the contribution of these modes to the electrons' acceleration is a negligible one. It is, however, expected that protons will be efficiently heated and their parallel temperature will grow anisotropic but this will make the object of our next investigations.

In the other limit of waves propagating perpendicular to the magnetic field, the free energy residing in the velocity anisotropy of plasma particles destabilizes the ordinary mode (Davidson 1983). The dispersion relation has been derived following the approach of Tautz & Schlickeiser (2006), and the growth rates of the unstable mode have been calculated for both small and large values of the Larmor radius. This is the filamentation Weibel-like instability driven by a bulk velocity anisotropy of counterstreaming plasmas enhanced or not by an intrinsic thermal anisotropy of plasma flows. The filamentation instability is inhibited in a magnetized plasma, but the effect of high-energy tails in the electron distribution functions is opposite to that found in Paper I for parallel waves: here, we have found that kappa populations can make the filamentation instability to grow faster whether the intrinsic thermal anisotropy of plasma flows is sufficiently low (see in Fig. 4). These results are in perfect agreement with those obtained for an unmagnetized plasma (Lazar et al. 2008b), and we conclude that only the filamentation two-streams driven instability (electromagnetic) is enhanced by the suprathermal tails, while the temperature anisotropy driven instability (Weibel) and the electrostatic two-stream instability are both inhibited in kappa-distributed plasmas.

Furthermore, two applications have been identified here for such counterflowing plasma structures developing in solar wind and flares and which are expected to be kappa-distributed. First, we have considered the solar wind outflows in the outer corona region and where the filamentation instability described above can be responsible for the 2D magnetic fluctuations detected (Stockem et al. 2006). The exact numerical growth rates have been displayed for two kappa-distributed populations, $\kappa = 2$ and 4 (see in Figs 4–6), and the aperiodic solutions obtained for large kappa spectra tend to approach the Maxwellian. In this case, as was shown above, the effect of suprathermal tails can be opposite to that obtained for parallel waves: the growth rates are higher and the instability faster than for Maxwellian plasmas (Fig. 4). But it is very important to note that the unstable wavenumbers extend to a markedly larger broadband, making this instability more likely to be found in space plasmas with anisotropic distributions of kappa-type.

In the second application, we have considered solar flares in the initial impulsive stage with a sufficiently large spectral index, $\kappa \gg 1$, and the distribution function have been approximated by a Maxwellian, thus allowing for exact numerical calculation of the growth rates using the method of Tautz & Schlickeiser (2006). In this case, typical solar plasma parameters show that the value of the streaming velocity has the most important influence, followed by the absolute value of the temperature and the temperature anisotropy, which only has a weak influence on the growth rates (see Figs 7–9). The overarching condition, however, is the background magnetic field strength, which enters the gyrofrequency that must not exceed a value of $\Omega_e \approx 0.1\omega_{p,e}$. Stronger ambient magnetic fields efficiently suppress the instability.

Therefore, the instability investigated here provides a method to create magnetic fields and thus to heat plasma. Because the instability is mediated by larger temperatures and magnetic field strengths, the mechanism is self-regulated and is able to keep a steady state as long as the counterstreaming is maintained. In the light of recent work, e.g. Tomczyk et al. (2007), Cirtain et al. (2007), that deals with the Alfvén waves in the solar corona and outflows, such waves are believed to be capable of providing a heating mechanism of the solar corona *and* are claimed to have been observed by several astronomers (see Cirtain et al. 2007 and references therein). Future work should, therefore, investigate the interplay of these unstable modes with the Alfvén waves in order to enlarge the understanding of the coronal heating processes.

ACKNOWLEDGMENTS

The authors acknowledge financial support from the Research Foundation Flanders – FWO Belgium, the Katholieke Universiteit Leuven through the fellowship F/07/061 and the Deutsche Forschungsgemeinschaft through the grant No. Schl 201/17-1. These results were obtained in the framework of the projects GOA/2009-009 (K.U.Leuven), G.0304.07 (FWO-Vlaanderen) and C 90347 (ESA Prodex 9). Financial support by the European Commission through the SOLAIRE Network (MTRN-CT-2006-035484) and SOTERIA (Collaborative project 218816 of FP7-SPACE-2007-1) is gratefully acknowledged. The numerical results were obtained on the HPC cluster VIC of the K.U.Leuven.

REFERENCES

Aschwanden M. J., 2004, Physics of the Solar Corona. Springer, New York
Bornatici M., Lee K. F., 1970, Phys. Fluids, 13, 3007
Cary J. R., Thode L. E., Lemons D. S., Jones M. E., Mostrom M. A., 1981, Phys. Fluids, 24, 1818
Cirtain J. W. et al., 2007, Sci, 318, 1580
Davidson R. C., 1983, in Rosenbluth M. N., Sagdeev R. Z., eds, Handbook of Plasma Physics. North-Holland Publishing Co. (Elsevier), Amsterdam, p. 519
Feldman W. C., Asbridge J. R., Bame S. J., Montgomery M. D., 1974, Rev. Geophys., 12, 715
Feldman W. C., Asbridge J. R., Bame S. J., Montgomery M. D., Gary S. P., 1975, J. Geophys. Res., 80, 4181
Fried B. D., 1959, Phys. Fluids, 2, 337
Gosling J. T., Bame S. J., Feldman W. C., McComas D. J., Phillips J. L., 1993, Geophys. Res. Lett., 20, 2335
Gradshteyn I. S., Ryzhik I. M., 1965, Tables of Integrals, Series and Products. Academic Press, New York
Lazar M., Schlickeiser R., Poedts S., Tautz R. C., 2008a, MNRAS, 390, 168 (Paper I)
Lazar M., Schlickeiser R., Shukla P. K., 2008b, Phys. Plasmas, 15, 042103
Lazar M., Dieckmann M. E., Poedts S., 2009a, J. Plasma Phys., online [doi:10.1017/S0022377809008101]
Lazar M., Schlickeiser R., Wielebinski R., Poedts S., 2009b, ApJ, 693, 1133
Lerche I., 1966, Phys. Fluids, 9, 1073
Leubner M. P., 2000, Planet. Space Sci, 48, 133
Leubner M. P., Viñas A. F., 1986, J. Geophys. Res., 91, 13, 366
Ma C., Summers D., 1998, Geophys. Res. Lett., 25, 4099
Mace R. L., Hellberg M. A., 1995, Phys. Plasmas, 2, 2098

Maksimovic M., Pierrard V., Riley P., 1997a, Geophys. Res. Let., 24, 1151
Maksimovic M., Pierrard V., Lemaire J. F., 1997b, A&A, 324, 725
Marsch E., Muhlhauser K. H., Schwenn R., Rosenbauer H., Pilipp W. G., Neubauer F. M., 1982, J. Geophys. Res., 87, 52
Miller J. A., 1991, ApJ, 376, 342
Miller J. A., 1997, ApJ, 491, 939
Montgomery M. D., Bame S. J., Hundhausen A. J., 1968, J. Geophys. Res., 73, 4999
Pierrard V., Maksimovic M., Lemaire J. F., 1999, J. Geophys. Res., 104, 17021
Pierrard V., Maksimovic M., Lemaire J. F., 2001, J. Geophys. Res., 106, 29305
Pilipp W. G., Miggenrieder H., Montgomery M. D., Muhlhauser K. H., Rosenbauer H., Schwenn R., 1987, J. Geophys. Res., 92, 1075
Pilipp W. G., Miggenrieder H., Montgomery M. D., Muhlhauser K. H., Rosenbauer H., Schwenn R., 1990, J. Geophys. Res., 95, 6305
Robinson P. A., 1988, Phys. Fluids, 31, 107
Salem C., Hubert D., Lacombe C., Bale S. D., Mangeney A., Larson D. E., Lin R. P., 2003, ApJ, 585, 1147
Schaefer-Rolffs U., Schlickeiser R., 2005, Phys. Plasmas, 12, 22104
Schlickeiser R., 2002, Cosmic Ray Astrophysics. Springer-Verlag, Berlin
Scudder J. D., 1992, ApJ, 398, 299 [ApJ, 398, 319]
Shizgal B. D., 2007, Astrophys. Space Sci., 312, 227
Stockem A., Lerche I., Schlickeiser R., 2006, ApJ, 651, 584
Stverak S., Travnicek P., Maksimovic M., Marsch E., Fazakerley A. N., Scime E. E., 2008, J. Geophys. Res., 113, A03103
Summers D., Ma C., 2000, J. Geophys. Res., 105, 15, 887
Summers D., Thorne R. M., 1991, Phys. Fluids B, 3, 1835
Tautz R. C., Schlickeiser R., 2006, Phys. Plasmas, 13, 062901
Thorne R. M., Summers D., 1991, Phys. Fluids B, 3, 2117
Tomczyk S., McIntosh S. W., Keil S. L., Judge P. G., Schad T., Seeley D. H., Edmondson J., 2007, Sci, 317, 1192
Treumann R. A., 1997, Geophys. Res. Lett., 24, 1727
Vasyliunas V. M., 1968, J. Geophys. Res., 73, 2839
Weibel E. S., 1959, Phys. Rev. Lett., 2, 83
Zaheer S., Murtaza G., 2007, Phys. Plasmas, 14, 022108
Zouganelis I., 2008, J. Geophys. Res., 113, A08111
Zouganelis I., Meyer-Vernet N., Landi S., Maksimovic M., Pantellini F., 2005, ApJ, 626, L117

APPENDIX A: DERIVATIVES OF THE DISTRIBUTION FUNCTION (1)

The partial derivatives of the distribution function (1), used in this paper and in Paper I, are shown here as follows:

$$\frac{\partial f_\kappa}{\partial v_\parallel} = -\frac{2}{\pi^{3/2}\theta_\perp^2\theta_\parallel}\,\frac{\Gamma(\kappa+2)}{\kappa^{5/2}\Gamma(\kappa-1/2)} \times\left\{\epsilon_1\,\frac{v_\parallel - v_1}{\theta_1^2}\,\left[1+\frac{(v_\parallel-v_1)^2}{\kappa\theta_1^2}+\frac{v_\perp^2}{\kappa\theta_\perp^2}\right]^{-\kappa-2} +\epsilon_2\,\frac{v_\parallel + v_2}{\theta_2^2}\,\left[1+\frac{(v_\parallel+v_2)^2}{\kappa\theta_2^2}+\frac{v_\perp^2}{\kappa\theta_\perp^2}\right]^{-\kappa-2}\right\} \tag{A1}$$

and

$$\frac{\partial f_\kappa}{\partial v_\perp} = -\frac{2v_\perp}{\pi^{3/2}\theta_\perp^4\theta_\parallel}\,\frac{\Gamma(\kappa+2)}{\kappa^{5/2}\Gamma(\kappa-1/2)} \times\left\{\epsilon_1\,\left[1+\frac{(v_\parallel - v_1)^2}{\kappa\theta_1^2}+\frac{v_\perp^2}{\kappa\theta_\perp^2}\right]^{-\kappa-2} +\epsilon_2\,\left[1+\frac{(v_\parallel+v_2)^2}{\kappa\theta_2^2}+\frac{v_\perp^2}{\kappa\theta_\perp^2}\right]^{-\kappa-2}\right\}. \tag{A2}$$

APPENDIX B: INTEGRAL IN EQUATION (8) FOR $Z \ll 1$

In order to evaluate the integral in equation (8), here we restrict to small wavenumbers, so that

$$z_e = \frac{k v_\perp}{\Omega_e} \ll 1 \tag{B1}$$

and according to Schlickeiser (2002), p. 207, $S(\alpha, z)$ from (9) simplifies as follows:

$$S(\alpha, z \ll 1) \simeq -\frac{1}{\alpha} + \frac{z^2}{2\alpha(1-\alpha^2)}. \tag{B2}$$

For the sake of simplicity, we consider symmetric counterstreams with $\epsilon_1 = \epsilon_2 = 1/2$, $v_1 = v_2 \equiv v_0$, $\theta_1 = \theta_2 \equiv \theta$. Inserting the distribution function (1) and using cylindrical coordinates, the integral in equation (8) becomes

$$\begin{aligned} I_1 &= \int \mathrm{d}^3 v\ [1+\alpha S(\alpha,z)]\ \frac{v_\parallel^2}{v_\perp}\,\frac{\partial f_e}{\partial v_\perp} \\ &= \frac{\Gamma(\kappa+2)}{\pi^{1/2}\theta_\perp^4\theta\kappa^{5/2}\Gamma(\kappa-1/2)}\,\frac{k^2}{\Omega_e^2-\omega^2}\int_{-\infty}^{\infty}\mathrm{d}v_\parallel\, v_\parallel^2 \\ &\quad\times\int_0^\infty \mathrm{d}v_\perp\, v_\perp^3\left\{\left[1+\frac{(v_\parallel-v_0)^2}{\kappa\theta^2}+\frac{v_\perp^2}{\kappa\theta_\perp^2}\right]^{-\kappa-2}\right. \\ &\quad\left.+\left[1+\frac{(v_\parallel+v_0)^2}{\kappa\theta^2}+\frac{v_\perp^2}{\kappa\theta_\perp^2}\right]^{-\kappa-2}\right\} \\ &= \frac{k^2v_0^2}{\omega^2-\Omega_e^2}\left[1-\frac{\kappa}{2\kappa-3}\,\frac{\theta^2}{v_0^2}\right] \\ &= \frac{k^2v_0^2}{\omega^2-\Omega_e^2}\left[1-\frac{v_T^2}{v_0^2}\right], \end{aligned} \tag{B3}$$

where $v_{T_1} = v_{T_2} \equiv v_T$ is given by equation (3). In this limit, there is no difference between plasmas with Maxwellian and kappa distributions.

APPENDIX C: INTEGRAL IN EQUATION (6) FOR LARGE $Z \gg 1$

In order to calculate the integral in equation (6) in the limit of large $z \gg 1$, we first proceed to the evaluation of the sum in equation (6):

$$S_1 \equiv \sum_{n=-\infty}^{\infty}\frac{nJ_n^2(z)}{\alpha-n} = J_0^2(z) - 1 - 2\alpha^2 S_2, \tag{C1}$$

where

$$S_2 \equiv \sum_{n=1}^{\infty}\frac{J_n^2(z)}{n^2-\alpha^2}. \tag{C2}$$

If we assume large $z \gg 1$,

$$J_n^2(z\gg 1) \simeq \frac{1}{\pi z}\left[1+\cos\left(2z-\frac{\pi}{2}-n\pi\right)\right] \tag{C3}$$

and

$$S_2 = \frac{1}{\pi z}\left[\sum_{n=1}^{\infty}\frac{1}{n^2-\alpha^2}+\sin(2z)\sum_{n=1}^{\infty}\frac{(-1)^n}{n^2-\alpha^2}\right]. \tag{C4}$$

The sums in equation (C4) can be further reduced as follows (Gradshteyn & Ryzhik 1965):

$$\sum_{n=1}^{\infty}\frac{1}{n^2-\alpha^2} = \frac{1}{2\alpha^2} - \frac{\pi}{2\alpha}\,\frac{\cos(\alpha\pi)}{\sin(\alpha\pi)}, \tag{C5}$$

$$\sum_{n=1}^{\infty} \frac{(-1)^n}{n^2-\alpha^2} = \frac{1}{2\alpha^2} - \frac{\pi}{2\alpha \sin(\alpha\pi)}, \tag{C6}$$

and then substituting equation (C4) in equation (C1), we find

$$S_1 = J_0^2(z) - 1 - \frac{1}{\pi z}\Bigg\{1 + \sin(2z) - \frac{\pi\alpha}{\sin(\alpha\pi)}\left[\cos(\alpha\pi) + \sin(2z)\right]\Bigg\}. \tag{C7}$$

J_0 can be also simplified as

$$J_0^2(z \gg 1) \simeq \left[\sqrt{\frac{2}{\pi z}}\cos\left(z - \frac{\pi}{4}\right)\right]^2 \simeq \frac{1}{\pi z}\left[1 + \sin(2z)\right], \tag{C8}$$

and the sum becomes

$$S_1(z \gg 1) = -1 + \frac{1}{z}\frac{\alpha}{\sin(\alpha\pi)}\left[\cos(\alpha\pi) + \sin(2z)\right]. \tag{C9}$$

Assuming $\alpha = \omega/\Omega_e \ll 1$, the sum S_1 simply approximates

$$S_1(\alpha \ll 1, z \gg 1) \simeq -1. \tag{C10}$$

Here, we again consider symmetric counterstreams described by the distribution function (1), and using equation (C10) the integral in equation (6) simplifies as follows:

$$\begin{aligned} I_2 &= -\int \mathrm{d}^3 v \, \frac{v_\parallel^2}{v_\perp}\frac{\partial f_e}{\partial v_\perp} \\ &= \frac{2\Gamma(\kappa+2)}{\pi^{1/2}\theta_\perp^4\theta\kappa^{5/2}\Gamma(\kappa-1/2)}\int_{-\infty}^{\infty}\mathrm{d}v_\parallel \, v_\parallel^2 \\ &\quad \times \int_0^{\infty}\mathrm{d}v_\perp \, v_\perp \Bigg\{\left[1 + \frac{(v_\parallel - v_0)^2}{\kappa\theta^2} + \frac{v_\perp^2}{\kappa\theta_\perp^2}\right]^{-\kappa-2} \\ &\quad + \left[1 + \frac{(v_\parallel + v_0)^2}{\kappa\theta^2} + \frac{v_\perp^2}{\kappa\theta_\perp^2}\right]^{-\kappa-2}\Bigg\} \\ &= \frac{\theta^2}{\theta_\perp^2}\left[1 + \left(2 - \frac{1}{\kappa}\right)\frac{v_0^2}{\theta^2}\right] \\ &= \frac{v_T^2}{v_{T_\perp}^2}\left[1 + \frac{2\kappa - 1}{2\kappa - 3}\frac{v_0^2}{v_T^2}\right]. \end{aligned} \tag{C11}$$

Note that in this limit, the integral exhibits a strong dependence on the spectral index κ.

This paper has been typeset from a TEX/LATEX file prepared by the author.